J. Water Environ. Nanotechnol., 6(2): 121-137 Spring 2021

ORIGINAL RESEARCH PAPER

Polyether Sulfone-Graphene Oxide- Polyvinyl Pyrrolidone Nanocomposite Adsorptive Membrane for Arsenic Removal from Wastewater

Nik-Rashida Nik-Abdul-Ghani, Siti-Syakirah Sulaiman, Amina Tahreen, Mohammed Saedi Jami*

Department of Biotechnology Engineering, Kulliyyah of Engineering, International Islamic University. Malaysia (IIUM), Jalan Gombak, 53100 Selangor, Malaysia.

Received: 2021-04-04 Accepted: 2021-04-27 Published: 2021-05-01

ABSTRACT

Arsenic contamination poses a major public health concern and harms the environment with its toxicity. Long-term exposure to a high concentration of arsenic is harmful to human health as well as environmental biodiversity. This study is aimed to fabricate and investigate the possibility of polyethersulfone-graphene oxide-polyvinyl pyrrolidone (PES-GO-PVP) nanocomposite adsorptive membrane and use it to enhance the removal of arsenic from wastewater. The nanocomposite membrane in this study was fabricated via the non-solvent induced phase separation (NIPS) method with the addition of polyvinylpyrrolidone (PVP) as a pore-forming agent. Based on the characterization results of GO through Fourier-Transform Infrared Spectroscopy (FTIR), X-ray diffraction (XRD), and Raman spectroscopy, the existence of a high quantity of oxygen-based functional groups with a high degree of oxidation was observed, which indicated that the GO was well-synthesized. The characterization of the nanocomposite membrane indicated that the addition of GO and PVP could impact the membrane hydrophilicity and mechanical stability. Three adsorption parameters (initial concentration of arsenic, pH, and contact time) were then optimized using a face-centered central composite design (FCCCD). The arsenic removal efficiency of 88.6 % was obtained with 55 mg/L of initial arsenic concentration, at pH 8 and 75 minutes of contact time between PES-GO-PVP membrane and the arsenic-contaminated wastewater. The Langmuir isotherm model fitted the equilibrium data, describing the monolayer adsorption mechanism that occurred on the surface of the nanocomposite membrane. Therefore, the results obtained in this study prove the suitability and promising potential of the GO modified membrane for the effective removal of arsenic through adsorption.

Keywords: *Graphene oxide-based membrane; characterization; adsorption; optimization; adsorption isotherm*

How to cite this article

Nik-Abdul-Ghani N.R., Sulaiman S.S, Tahreen A., -Saedi Jami M. Polyether Sulfone-Graphene Oxide- Polyvinyl Pyrrolidone Nanocomposite Adsorptive Membrane for Arsenic Removal from Wastewater. J. Water Environ. Nanotechnol., 2021; 6(2): 121-137. DOI: 10.22090/jwent.2021.02.003

INTRODUCTION

Heavy metal pollution such as arsenic contamination is one of the global health concerns. There are several regions in the world where arsenic contamination in drinking water is significant as arsenic exists naturally in their groundwater [1]. Industrial activities tend to also contribute to arsenic contamination to the water source [2-4]. Treatment for arsenic removal in wastewater is required to reduce the risk of health hazards and to preserve aquatic life. According to the World Health Organization (WHO) report in 2018, long-term exposure to a high level of arsenic in drinking water can cause skin diseases, hyperkeratosis, pulmonary and cardiovascular diseases. Existing technologies

* Corresponding Author Email: *saedi@iium.edu.my*

such as ion exchange, coagulation-flocculation, electrochemical treatment, chemical precipitation, and adsorption have been explored and utilized to remove heavy metals from wastewater. Many studies explored bioremediation with algae for removing arsenic [5]. However, the major drawbacks of most of these methods are the production of toxic by-products, a need for a regular exchange of expensive components, and incomplete pollutant removal [6-9]. Among the listed methods, adsorption has been proven to be one of the simplest and effective treatments and the most cost-effective for sustainable pollutant removal [2]. In order to synthesize enhanced adsorbents for arsenic removal, the work of Imran et al. [10] and Iqbal et al. [11] are notable. However, a membrane filtration process is necessary to follow up the adsorption process to remove the adsorbed pollutants.

Membrane technology with a dual function of adsorption and filtration had been rapidly studied due to its potential of efficiently removing heavy metals from wastewater [12]. Therefore, adsorption along with filtration through an efficient adsorptive membrane is an added advantage in the wastewater treatment system reducing the need for an additional filtration step. Hence, this study explores the synthesis and application of an effective adsorptive membrane.

In the wastewater treatment industry, membrane separation techniques such as microfiltration, ultrafiltration, and nanofiltration are widely used as pre-treatment and subsequent treatment of wastewater and seawater desalination processes [13]. Limitations that are faced in these processes include that the membrane used is prone to fouling and low surface hydrophilicity, especially in treating wastewater contaminated with heavy metals [8]. Modification of polymeric membranes with nanomaterials is being studied extensively due to the great sorption ability between nanomaterials and heavy metals, and the resulting high surface area, high porosity, and interconnected porous structure [2,14,15]. The use of nanomaterials to enhance the polymeric membrane properties has attracted researchers to conduct several studies in fabricating the optimum adsorptive membrane for removing heavy metals from wastewater. Graphene; a nanomaterial, is a two-dimensional, hexagonal lattice made up of carbon atoms on the atomic scale [16]. Naturally, graphene is hydrophobic but when narrow pores are constructed in it, rapid water permeation can take place [17]. However, limitations in nanoporous graphene's mechanical stability are a major drawback as water permeability increases with increased pore quantity. Alternatively, GO, a highly oxidized form of graphene, has been studied due to its easy dispersion in an aqueous solution as the oxygen moieties make GO hydrophilic [17]. GO-based materials have been extensively used for wastewater treatment due to enhanced active sites with the oxygen-based functional group present on the surface that increases its adsorption capacity [18]. GO can be produced by chemically exfoliating graphite without the use of complex apparatus and catalysts [11]. Therefore, additional purification step such as acid treatment is not required as graphene is free of catalyst impurities. Besides, with the attachment of strong functional groups namely hydroxyl and carboxyl groups on the GO surface, the membrane becomes a potential adsorbent for the removal of heavy metals.

Polyethersulfone (PES) is one of the materials that is widely used in the fabrication of membranes for wastewater treatment and medical applications due to its excellent mechanical and thermal properties in both hot and wet environments [19]. The use of polyvinylpyrrolidone (PVP), as an additive in polymeric membranes, has also been explored due to its high compatibility properties with solvents, pore expansion capacity, and ability to improve membrane hydrophilicity [20,21]. Not many studies have been undertaken to explore the ability of PES-PVP membrane enhanced with GO to explore the adsorption ability for removing heavy metals, namely arsenic. Furthermore, the lack of information on the interaction between the membrane and the adsorbate remains a significant challenge to our understanding of the resulting adsorption mechanisms of the PES-GO-PVP adsorptive membrane. Therefore, this study aims to fabricate and characterize the PES-GO-PVP nanocomposite adsorptive membrane and use it to enhance arsenic removal from wastewater and to study the governing adsorption mechanism. The membrane fabrication was carried out using the non-solvent induced phase separation (NIPS) method. Then, the optimization of adsorption parameters, and adsorption isotherms were investigated on synthetic wastewater solution containing arsenic to explain the mechanism of arsenic ions adhering onto the modified PES-GO-PVP nanocomposite adsorptive membrane when influenced by critical experimental factors such as pH, contact time, and initial arsenic concentration.

MATERIALS AND METHOD

Chemicals

Graphite powder (particle size < 50 μm), sodium nitrate ($NaNO_3$; 99%), sodium hydroxide (NaOH), hydrogen peroxide (H_2O_2; 30% aqueous solution), sulphuric acid (H_2SO_4; 98%), hydrochloric acid (HCl; 37%), sodium arsenite ($NaAsO_2$; 99%), potassium dichromate ($K_2Cr_2O_7$; 98%) and polyvinylpyrrolidone (PVP) (MW = 40,000 g mol−1) were utilized for pore formation in the membrane fabrication and N, N- dimethylformamide (DMF, 99.5%) was used as solvent. These chemicals were purchased from R&M Chemicals, Canada. Potassium permanganate ($KMnO_4$; 99%), was purchased from Chemiz, Malaysia. The design of the experiment, process optimization, and statistical analysis was carried out using Design Expert® software version 6.0.8 (STAT-EASE Inc. Minneapolis, USA).

Graphene oxide (GO) synthesis

GO was synthesized following Hummer's method with some modifications [22]. 115 mL of H_2SO_4 was added to 5 g of graphite and 2.5 g $NaNO_3$ in a 2-liter beaker. Then, the mixture was stirred for 120 minutes at room temperature at a constant speed of 500 rpm. Next, the mixture was relocated to an ice bath to decrease the temperature to below 10 °C. After that, 20 g of $KMnO_4$ was added slowly while stirring the mixture at 500 rpm speed for 2 h. Then, the temperature was raised to 35 °C and stirred for 1 h followed by the dilution of the mixture using 230 mL of deionized water at constant temperature (90 °C) and was stirred for 1 h and continued with another 250 ml of deionized water for further dilution. Next, the temperature was decreased to 60 °C before 10 mL of 30% H_2O_2 was added to the mixture to remove the remaining $KMnO_4$. Finally, for purification, the mixture was washed using 5% HCl followed by deionized water by centrifugation method (Thermo Scientific Sorvall X1R Centrifuge, USA). The solution was washed consecutively to get the near-neutral pH value. After that, the sediment from the centrifugation process was freeze-dried to obtain GO in powdered form with fine dark-brownish color.

Fabrication of membrane by phase inversion technique

Dope polymer composition was prepared to fabricate the PES-GO-PVP membrane. 0.5 wt.% of GO was mixed with dimethylformamide (DMF) solvent and the solution was sonicated for 1 hour at 20 °C. Then, 17 wt.% of PES and 0.5 wt.% of PVP were added into the solution and mixed using a magnetic stirrer for 24 hours [23]. The PES-GO-PVP membrane was fabricated using the NIPS technique. First, the stainless-steel casting blade and glass plate (210 × 297 × 5 mm) were sterilized with 70% ethanol. Then, the casting solution was poured on a glass plate to cast the membrane of 0.2 mm thickness. After 15 seconds of pre-evaporation at room temperature, the glass plate was immersed into the non-solvent bath (coagulation bath) and kept in the container for up to 24 h. The fabricated membrane was kept in a container with deionized water and stored in a chiller, before its usage.

Characterization of GO and membrane

Characterization of the synthesized GO powder and membrane was achieved by conducting FTIR, Raman spectroscopy, XRD, and SEM analyses. Analysis of the functional groups in the samples was performed using a Nicolet iS50 FTIR spectrometer (Thermo Scientific, Massachusetts, US). The Raman spectra were obtained by Renishaw inVia™ Raman Microscope (Gloucestershire, UK) with a laser power of 50%, 785 nm edge wavelength. Powder X-ray diffraction (XRD) spectroscopy was carried on D2 Phaser 2nd Gen, Bruker and operated with 0.25 s of time/step at 30 kV using *Cu Kα* radiation (wavelength = 1.5406 Å). The surface and cross-section morphology of the GO and membrane were observed by SEM (JSM-IT 100, Jeol, Japan) after coating with a thin gold film using a sputter coater device (Q-SC7620, Quorum Tech Ltd. London). To reveal the cross-section images under SEM, liquid nitrogen was used to immerse the membranes for several seconds and then cut with a stainless-steel knife before observation through SEM. To determine the membrane mechanical stability, the dumbbell-shaped membrane samples (bare PES and PES-GO-PVP) were inserted into the grips fitted with cardboard and epoxy glue to maximize the contact adhesion with samples using a universal tensile machine (AGS-X Series, Shimadzu, Japan). The speed was set at 1 mm/min. The optimal amount of GO for introduction in the nanocomposite membrane and the study of membrane hydrophilicity has been previously reported [24].

Standard curve preparation

A standard curve or also known as a calibration

Table 1. Range of values for each factor

Factors	Units	Range of values	
		Low	High
Initial concentration of arsenic	mg/L	10	100
pH	-	4	12
Contact time	min	10	140

curve is required to relate absorbance with substance concentration, which is arsenic concentration in this work. A linear relationship between the physical quantities is required to find the final concentration of the treated sample. First, sodium arsenite ($NaAsO_2$) stock solution was prepared by dissolving 0.5 g of sodium arsenite with 500 ml of deionized water. A set of arsenic concentrations (in the range of 10 to 100 mg/L) was prepared for the standard curve. 0.01 g of potassium dichromate ($K_2Cr_2O_7$) was added to 100 ml deionized water and was used as a coloring agent to the arsenic solution for absorbance reading. The absorbance readings were taken using a UV-Vis spectrophotometer at a wavelength value of 430 nm. The graph for the standard curve was then generated as shown in Fig. 6.

Design of experiment

Response Surface Methodology (RSM) was utilized to design the batch adsorption experiment. The design of the experiment was performed using Design-Expert 6.0.8 software in which the face-centered central composite design (FCCCD) method was applied for its effectiveness in the optimization of the adsorption parameters. Three factors were selected to study the effects of parameters namely initial arsenic concentration, pH, and contact time on the percentage of arsenic removal from synthetic wastewater. The range of values for each factor is selected based on the previous report [3] and shown in Table 1. Percentage removal (%) was chosen as the response variable. 20 experimental runs were carried out in total.

Batch adsorption test

The batch adsorption test was performed to investigate the combined effect of the three parameters which are the initial concentration of arsenic, pH, and contact time. By conducting a batch adsorption test, the ability of the fabricated nanocomposite adsorptive membrane to remove arsenic was observed. It was carried out based on the 20 runs of experiments generated by Design-Expert 6.0.8 software. First, the initial concentrations of arsenic (10, 55, and 100 mg/L) with a final volume of 100 ml were prepared by diluting 1000 ppm arsenic stock solution with deionized water in a 250 ml conical flask. The pH value was then adjusted to pH 4, 8, and 12 using 1 M of NaOH and 3% of HCl. The membrane was cut into small pieces (with a total weight of 0.4 g) with a dimension of 1.5 × 1.5 cm squares and added into each conical flask. A laboratory shaker was used to agitate the mixture at 250 rpm for the contact times of 10, 75, and 140 minutes. Then, the sample was extracted and measured for its absorbance using UV-Vis Spectrophotometer to obtain the final arsenic concentration. The percentage removal was calculated using Equation (1).

$$Removal(\%) = \frac{C_0 - C_f}{C_0} x100 \quad (1)$$

Where C_o is the initial concentration of arsenic, while C_f is the final concentration of arsenic.

Adsorption isotherm

The resulting adsorption isotherm in the adsorption process was identified after obtaining the optimum conditions from the design of the experiment (DOE). 100 ml of varying initial concentrations of arsenic (20, 40, 60, 80, and 100 mg/L) were prepared in each conical flask. The pH value was calibrated to a fixed pH value of 8. The 0.4 g weighted membrane was added to the solution and the mixture was agitated at 250 rpm for 75 minutes. The treated sample was then extracted, and the absorbance reading was taken to determine the final concentration. Two isotherm models were used in this work to study the adsorption mechanism, namely Langmuir and Freundlich. The linear regression value, R^2 was calculated for both models to determine the model with the best fit.

The Langmuir isotherm assumes monolayer adsorption onto an adsorbent surface, and is expressed in Equation (2):

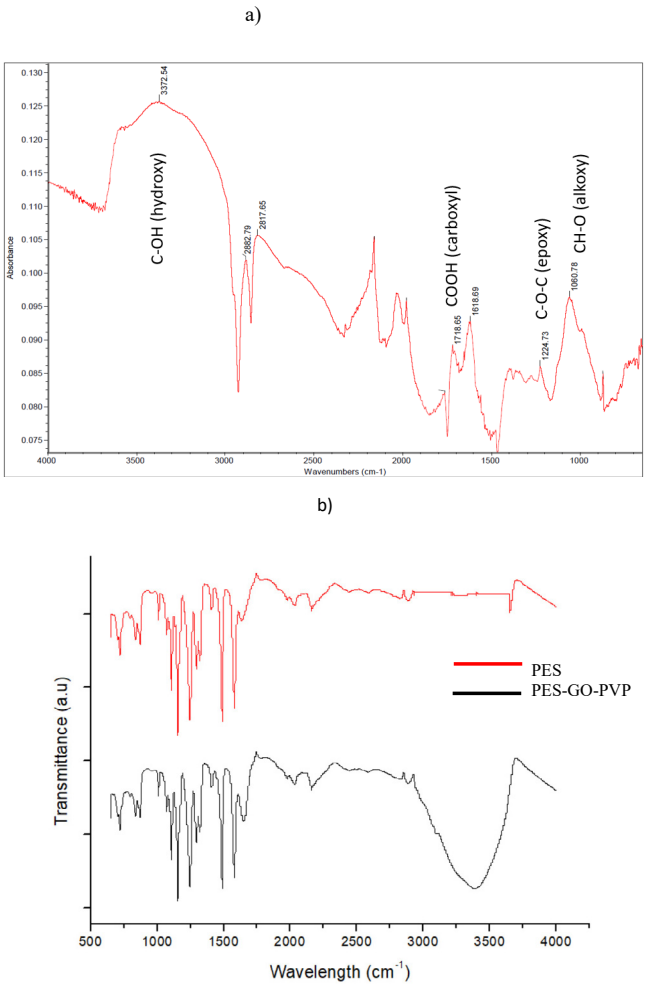

Fig. 1. FTIR spectrum of a) powder form of GO and b) bare PES and PES-GO-PVP membrane

$$\frac{1}{q_e} = \left[\frac{1}{q_{max} K_L}\right]\frac{1}{C_e} + \frac{1}{q_{max}} \quad (2)$$

where C_e is the solute concentration at equilibrium (mg/L), q_e is the corresponding adsorption capacity (mg/g), q_{max} is the maximum adsorption capacity (mg/g) and K_L is the Langmuir isotherm constant (L/mg) [25]. By plotting $1/q_e$ against $1/C_e$, the values of Langmuir constants, K_L, and q_m, can be calculated.

The Freundlich isotherm model, which describes multilayer adsorption, is the earliest known relationship describing non-ideal and reversible adsorption [25]. The linear form of the Freundlich model is shown in Equation (3):

$$\log q_e = \log K_F + \frac{1}{n} \log C_e \quad (3)$$

where K_F and n are constants that determine the adsorption capacity and intensity, respectively [16]. By plotting $\log(q_e)$ against $\log(C_e)$, both Freundlich constants of K_F and n can be calculated.

RESULTS AND DISCUSSION

Physicochemical Characterization of GO

Several characterizations of GO were conducted to confirm whether GO was well synthesized using FTIR, Raman spectroscopy, XRD, and SEM. The details of the results are discussed in the following sub-sections.

FTIR Analysis

The FTIR spectrum for GO is presented in Fig. 1a). The FTIR spectrum of GO exhibits the presence of functional groups such as hydroxyl, carboxyl, and epoxy. The highest band is at 3372.54 cm^{-1} that shows the existence of the hydroxyl (–OH) group which contributes to the hydrophilicity of GO. At 2882.79 cm^{-1}, the peak depicts the aliphatic C-H bond of GO. Meanwhile, peak 2817.65 cm^{-1} represents the C-H bond stretch off carboxyl group, C=O and the 1718.65 cm^{-1} peak shows the presence of carboxyl group (-COOH). The peak of 1618.69 cm^{-1} shows the double bond of (–C=C). The epoxy group (C-O-C) was located at 1224.73 cm^{-1} and the lowest peak of 1060.78 cm-1 represents the alkoxy group (–CH–O). This result agrees with other commercialized GO and several findings of synthesized GO, which also contained carboxyl, epoxy, and hydroxyl groups [22,26,27]. The functional groups with a high oxygen content, with hydroxyl and carboxyl groups, could be attributed to the fact that the GO was successfully oxidized during GO synthesis [22]. These polar oxygen functional groups in GO provide strong hydrophilic property, which contributes to the good dispersibility of GO in water and other solvents [27]. Moreover, the formation of epoxy groups in GO synthesis along with the hydroxyl and carboxyl groups is the result of an increase in the oxidation process [28].

The wavenumbers of 2817.65 cm^{-1} and 1618.69 cm^{-1} reveal the existence of aliphatic and aromatic bonds of GO, respectively. The aromatic ring of the adsorbate molecule, commonly acting as an electron acceptor, has been reported to improve the adsorption process [29,30]. The presence of the carboxyl group, which is represented by the wavenumber 1718.65cm^{-1}, indicates the mechanism of exfoliation that occurred due to CO_2 expansion during the rapid heating process [22,31]. The graphitic structures were exfoliated to allow the entrance of oxygen during the oxidation process [31].

The characteristic peaks of PES structures observed through FTIR analysis include a benzene ring, ether, and sulphone bond (3000-3300 cm^{-1}). The FTIR spectra of PES-GO-PVP nanocomposite membranes were found to be similar to bare PES membranes with an additional broader O-H peak at around 3391 cm^{-1}. The band at 1651 cm^{-1} is assigned to the vibrations of the adsorbed water molecules and the contributions from the vibration of aromatic C=C. This specifies that the composite PES membrane is more hydrophilic as compared to the bare PES membrane [32] (7). As GO was added, the O-H stretching peak became wider and stronger. The FTIR spectra of PES-GO-PVP composite membranes confirm the presence of GO peak, which further indicates the effective incorporation of GO into the PES matrix.

Raman Spectroscopy Analysis

Under Raman spectroscopy, GO is characterized by a G band at a spectrum attributed to the E2g phonon of the sp^2 carbon atoms and a D band which represents the breathing mode of k points phonon of A1g symmetry [33]. The existence of the D band indicates the disorder from certain defects including π-π interaction and amorphous carbon species [22,33]. The quality of the product and oxidation degree of GO can be reflected in Raman spectra by the relative intensity ratio of D peak to G peak (ID/IG ratio), which is a high-intensity ratio indicating high oxidation. From the result displayed in Fig. 2, ID/IG ratio value is shown as 1.18 where the D band is at 1339 cm^{-1} and the G band is at 1584 cm^{-1}.

XRD Analysis

From the XRD graph analysis, the graphite sample showed a peak of 26.44° corresponding to d = 3.35 nm and from the GO sample this peak has disappeared and the peak of produced GO is at 10.29° with the value of d-spacing is 8.59 nm (Fig.3). This result indicated that the oxidation of graphite to graphene oxide was successful, where the diffraction peak of graphene oxide shifted from 26.44° to 10.29° where the introduced functional groups on GO increased the distance between the layers, therefore, increasing the d-spacing value. This result agrees with previous studies which also reported that the XRD pattern of the graphite exhibited a diffraction peak at 2θ approximately 27° which is equivalent to an interlayer spacing (d-spacing = 0.34 nm) [28,34,35]. When the oxidation of graphite occurred, the diffraction pattern of graphite (27°) disappears due to the lattice distortion during oxidation reaction with an increase in the spacing between the graphene layers, followed by the peak shift to around 10.0 -11.4° corresponding to oxidation of graphite to GO [28,36]. Hence, the XRD analysis in this work proves that the graphite was fully oxidized to form GO and no graphite trace on the XRD

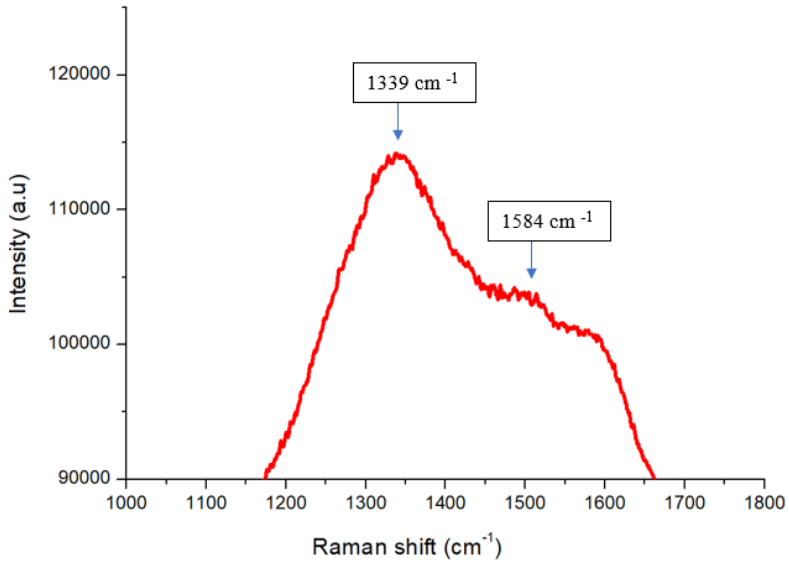

Fig. 2. Raman spectra of produced GO

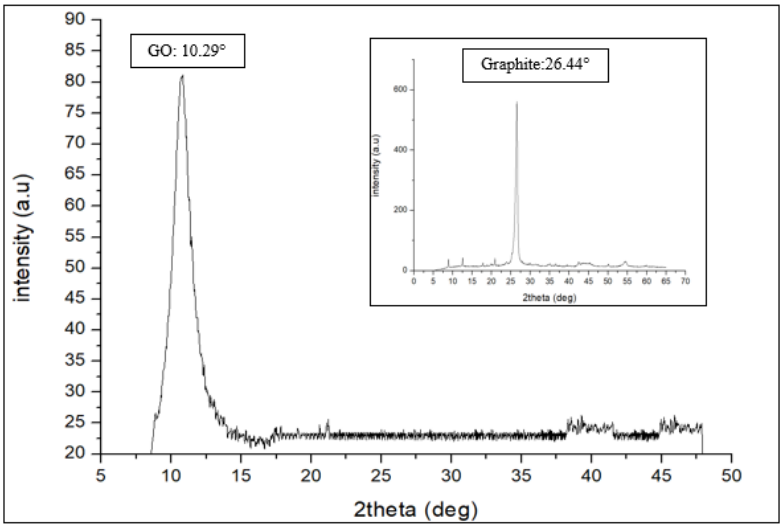

Fig. 3. XRD peak for graphite and GO.

pattern of GO was observed. The diffraction pattern and interlayer spacing value of GO were within the range in the previously reported studies [22,28,37].

SEM Analysis

Theoretically, GO has a larger surface area, higher solubility, as well as the capability of surface functionalization, which opened up a lot of possibilities for nanocomposite materials [38]. . The SEM analysis of GO, is shown in Fig. 4.

The SEM micrographs of GO synthesized by a modified Hummers process in Fig. 4 clearly show that GO is made up of randomly aggregated and crumpled areas, as well as wrinkled and folded areas on the GO surface in 1μm image scale. This result confirms that the graphite was exfoliated thoroughly throughout the oxidation process to produce GO [39,40]. The SEM morphology also indicates that the GO was thicker at the edges due to the hydroxyl and carboxyl functional groups [41]. These oxygenous functional groups (–OH-

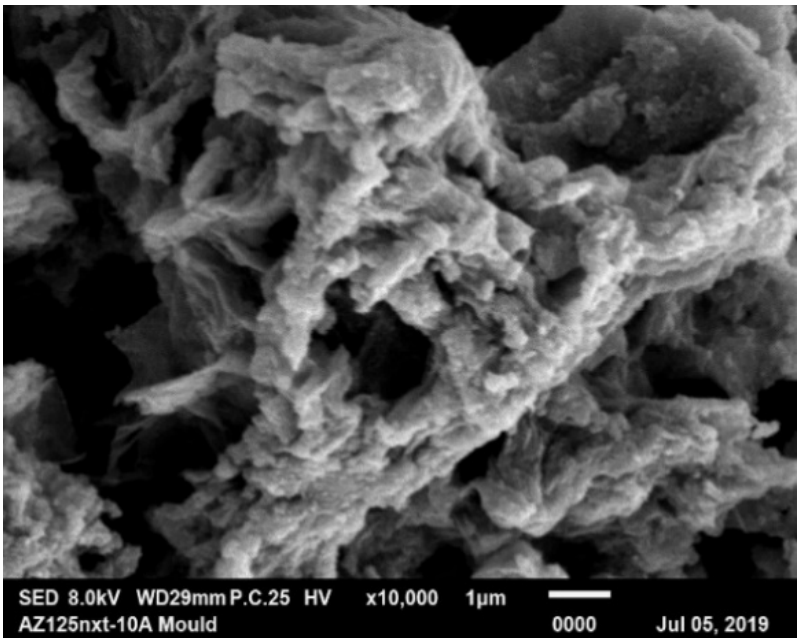

Fig. 4. SEM images of ×10 000 magnification of produced GO

or –COOH-) were the key factors that enhanced the adsorption process of metal ions where the adsorption affinity increased using electrostatic interaction, ion exchange, and surface complexation mechanisms [42]. It was reported that the oxygen-containing functional groups positioned at the edges of GO, mainly contributed to the surface complexation where the adsorption process is governed by chemical adsorption between lead ion and GO [42,43]. Moreover, the folded areas on the GO surface considerably influence the membrane's performance in terms of water uptake, mechanical properties, and proton conductivity due to the formation of interfacial hydrogen bond between the oxygen-related functional group in GO and polymer which then could lead to proton diffusion [40].

Characterization of membrane

Scanning electron microscopy (SEM) was used for analyzing the surface morphology of the fabricated membrane which were bare PES and PES-GO-PVP membranes. The surface and cross-section morphology of the bare PES showed a spongy-like porous structure (Fig. 5a and b). In Fig. 5c, the surface of the PES-GO-PVP membrane shows the monodispersed GO nanoparticles on the membrane surface while in Fig. 5d the cross-section morphology of PES-GO-PVP nanocomposite demonstrated the existence of the asymmetric structure with the thin dense top layer and finger-like structure with porous sublayer. The addition of GO and PVP increased the hydrophilicity of the membrane and improved the membrane adsorption performance [44,45].

Mechanical stability

A tensile test was performed to determine the mechanical stability of the PES-GO-PVP membrane. Mechanical stability is a crucial property of the membrane as it determines its ability to withstand the high pressure of the working conditions.

In Fig. 6, the PES membrane exhibits 1.33 MPa of ultimate strength (in terms of stress). This value is slightly low compared to the PES hollow fiber membrane (1.45 MPa) from the previous finding [46] but a higher value than the PES membrane studied by Mataram et al. [47] which is 0.523 MPa. For the PES-GO-PVP nanocomposite membrane, the ultimate strength is 1.45 MPa which is slightly higher than that of the bare PES. This suggests that the synergistic effects of the GO and PVP nanocomposite led to a more uniform dispersion in the dope solution and therefore, is more covalently bonded to the PES matrix [48]. This value was comparable with the PES-GO membrane which falls in the range of 0.84 – 2.55 MPa [49]. However,

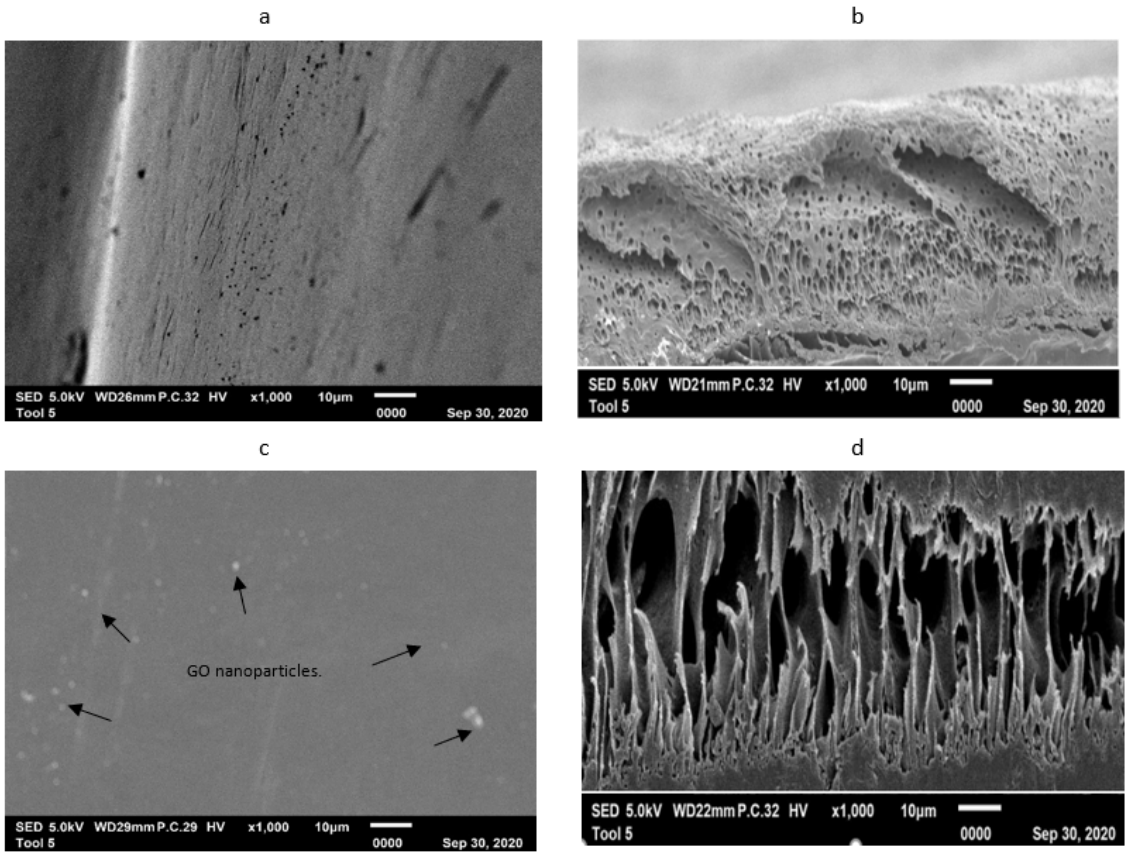

Fig. 5. SEM image of surface and cross-section of (a, b) PES membrane and (c, d) PES-GO-PVP adsorptive membrane. The white dots on the surface of the PES-GO-PVP membrane are the monodispersed GO nanoparticles.

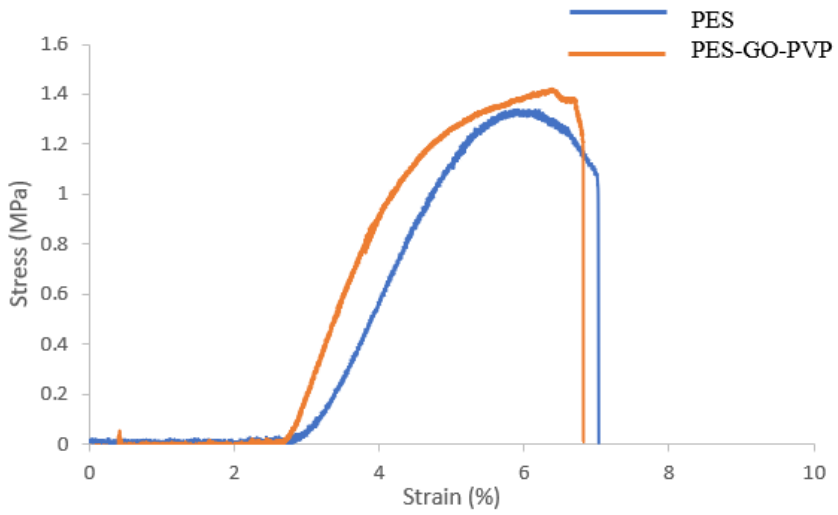

Fig. 6. Tensile strength of bare PES and PES-GO-PVP membranes plotted as stress vs strain.

Table 2. Concentration and absorbance reading for standard curve.

Concentration of arsenic (mg/L)	Absorbance
10	0.130
20	0.131
30	0.137
40	0.143
50	0.151
60	0.155
70	0.157
80	0.162
90	0.168
100	0.177

Table 3. Percent removal of arsenic for 20 runs of experiments.

Run	Contact time	pH	Initial concentration, C_o (mg/L)	Final concentration, C_f(mg/L)	Percent removal (%)
1	75	12	55	38.6	42.5
2	10	4	100	93.6	6.8
3	75	8	55	32.7	68.3
4	140	12	10	7.9	27.1
5	10	4	10	9.3	7.2
6	10	12	100	84.2	18.7
7	140	4	10	9.4	6.5
8	75	4	55	35.8	53.7
9	75	8	55	29.2	88.6
10	75	8	55	30.7	79.4
11	75	8	55	30.5	80.3
12	10	12	10	9.3	7.4
13	75	8	55	30.6	79.7
14	10	8	55	39.8	38.3
15	75	8	55	29.6	85.8
16	140	12	100	80.1	24.9
17	140	8	140	34.3	60.4
18	75	8	75	6.0	67.3
19	75	8	75	70.4	42.1
20	140	4	140	92.9	7.6

other findings on the tensile strength of PES-GO and PSF-GO nanocomposite showed relatively higher values, which were 11 MPa and 4.06 MPa, respectively. The differences in the tensile strength values were due to the low molecular weight (75kDa) of the utilized PES in this work, thus, indicating that the mechanical properties commonly depend on many factors such as chain structure, molecular weight, and crystallinity [50].

Standard curve for arsenic *analysis*

The absorbance reading for the concentrations of arsenic ranging from 10 to 100 mg/L was measured using a UV-Vis spectrophotometer as tabulated in Table 2.

From the tabulated data of concentration and absorbance readings in Table 2, a standard curve, or also known as a calibration curve, was generated. The graph shows the relationship between the arsenic concentration and its corresponding absorbance. Based on the graph in Fig. 6, the final concentration of arsenic can be obtained from Equation (4):

$$y = 0{\cdot}0005\,x + 0{\cdot}1227 \quad (4)$$

where y represents the absorbance value and x is the corresponding arsenic concentration. The regression value obtained was 0.9848, and as it is approaching 1, the reliability of the standard curve is proven.

Batch adsorption test

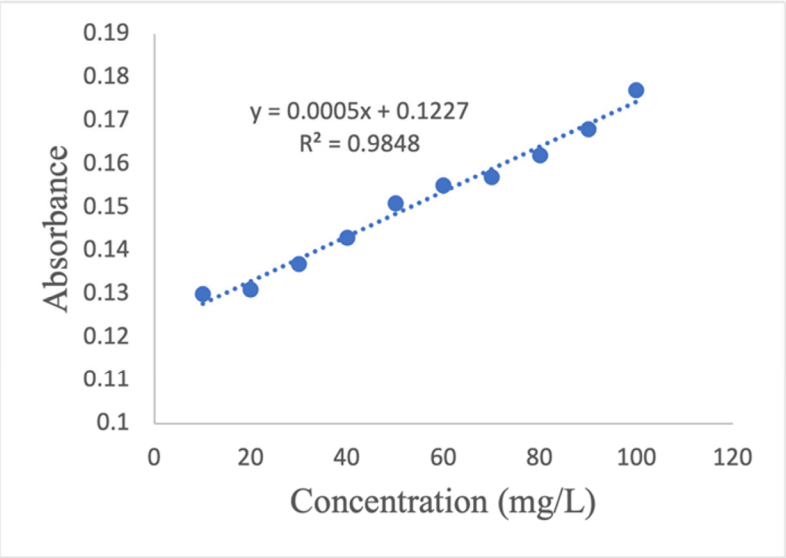

Fig. 7. Standard curve for arsenic.

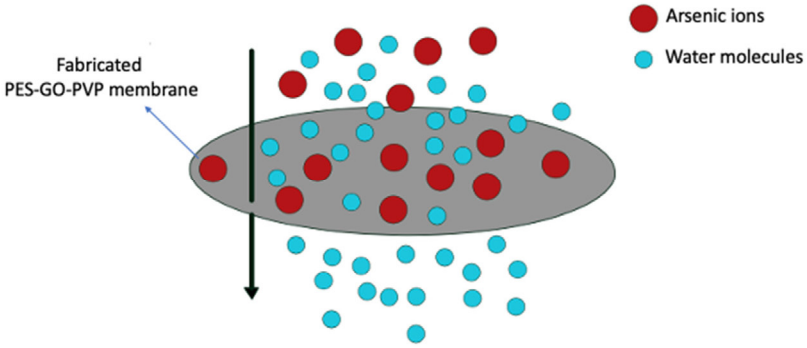

Fig. 8. Schematic representation of arsenic removal through PES-GO-PVP membrane adsorption. Adapted from [56].

The percentage removal for 20 runs of batch adsorption experiments was calculated and summarized (Table 3). The highest arsenic percentage removal of 88.6% was obtained at run number 9, where the initial arsenic concentration was 55 mg/L at pH 8 and contact time was 75 minutes. Arsenic removal efficiency increased from 10 mg/L to 55 mg/L of initial concentration and then decreased gradually as the initial concentration of arsenic increased up to 140 mg/L. This was due to the non-availability of active binding sites on the surface of the adsorbents, and it had reached the equilibrium state [3]. This phenomenon is delineated in the adsorption isotherm graph as shown in Fig. 10 where the adsorption capacity increases proportionally with the initial arsenic concentration until it reaches a plateau at 60 mg/L. pH is the most important factor to investigate metalloid speciation and sorption. The ionic charge of arsenic ions, GO nanoparticle and nanocomposite membrane differs at different pH conditions. At lower pH (pH 4) the arsenic removal was lower compared to pH 8, indicating that the adsorption of arsenic was more favorable in alkaline solution. This was due to the high amount of hydroxyl ions in an alkaline solution that increases the interaction between the functional groups on the nanocomposite membrane and arsenic ions [51]. Notably, at pH 12, the removal rate of arsenic was lower than that of pH 8. This result was most likely caused by the deprotonation rate of GO embedded in the nanocomposite membrane, which results in greater electrostatic repulsion and weak interaction among the nanocomposite adsorptive

Table 4. Analysis of variance (ANOVA) values.

Source	Sum of Squares	DF	Mean Square	F Value	Probability > F	
Model	15989.81	6	2664.97	28.44	<0.0001	significant
A	23.72	1	23.72	0.25	0.6233	-
B	150.54	1	150.54	1.61	0.2272	-
C	231.36	1	231.36	2.47	0.1401	-
A^2	862.88	1	862.88	9.21	0.0096	-
B^2	1625.67	1	1625.67	17.35	0.0011	-
C^2	1462.81	1	1462.81	15.61	0.0017	-
Residual	1218.13	13	93.70	-	-	-
Lack of fit	973.83	8	121.73	2.49	0.1648	Not significant
Pure error	244.29	5	48.86	-	-	-
Cor total	17207.94	19	-	-	-	-

membrane, GO nanoparticles, and arsenic ions as reported in several studies[52,53]. The adsorption capacity increased with the contact time, and the equilibrium was reached after 75 minutes when the highest arsenic percentage removal was achieved. Then, increasing contact time from 75 to 140 minutes led to a decrease in adsorption capacity. As time progresses, the surface of the nanocomposite adsorptive membrane becomes saturated with arsenic, and the adsorption equilibrium that was achieved, causes the percentage removal to decrease gradually [54,55]Fig. 7 depicts a schematic diagram of arsenic adsorption on the PES-GO-PVP membrane surface.

Statistical analysis

The percentage removal for arsenic was evaluated based on the response generated by Design-Expert software. The result of analysis of variance (ANOVA) was used to determine which model gave the best data fit. Table 4 shows the ANOVA and optimization conditions for the removal of arsenic from the PES-GO-PVP nanocomposite adsorptive membrane. The statistical significance of mean square ratio variation due to regression and residual errors was evaluated using the ANOVA technique. It was observed that some factors exhibited significant effects ($p<0.05$), while others were attributed to non-significant effects ($p>0.10$). The effects of parameter *A* on parameters *B* and *C* were observed. The tabulated results showed that factors *B* and *C*, which are pH and initial concentration, respectively, are significant model terms with high regression values. Meanwhile, the insignificant factor A (contact time) does not affect the output significantly. The model equation which is in the quadratic form presented a high R^2 of 0.9292 showing that 92.92% of the variations in arsenic removal efficiency could be explained by the independent variables: contact time, pH, and initial arsenic concentration. Moreover, the model depicted that the predicted R^2 of 0.7869 was in reasonable agreement with the adjusted R^2 value of 0.8965, which indicated that the model developed was successful. Adeq. Precision is a ratio of the signal to noise where a ratio greater than 4 is desirable. The ratio obtained was 13.152, hence, indicating an adequate signal that this model was suitable to navigate the design space. The CV value is a measure of residual data variation relative to the size of the mean. The higher the value of CV%, the less reliable are the experimental results. The model in this study showed 21.69% for CV, therefore, proving the reliability of the model.

Fig. 9 a) shows the graph of predicted values against the actual values where the closeness of the points towards attaining linearity verifies that the values are in relative agreement with each other. A straight line with well-distributed data can be observed showing that it has a reasonable agreement between experimental and predicted data. Graph for normal probability plot in Fig. 9 (b) shows data points scattering along the line which follows a normal distribution. Both plots of the graph in Fig. 9 (c) and (d) show a random scatter of points across the graph denoting similarity between predicted and experimental data.

Adsorption isotherm

The adsorption isotherm model was used to investigate the distribution of adsorbate molecules at equilibrium between the solid and liquid phases. Langmuir and Freundlich's linear models are commonly used for solid or liquid systems. Both Langmuir and Freundlich equilibrium data were determined and the estimated isotherm parameters

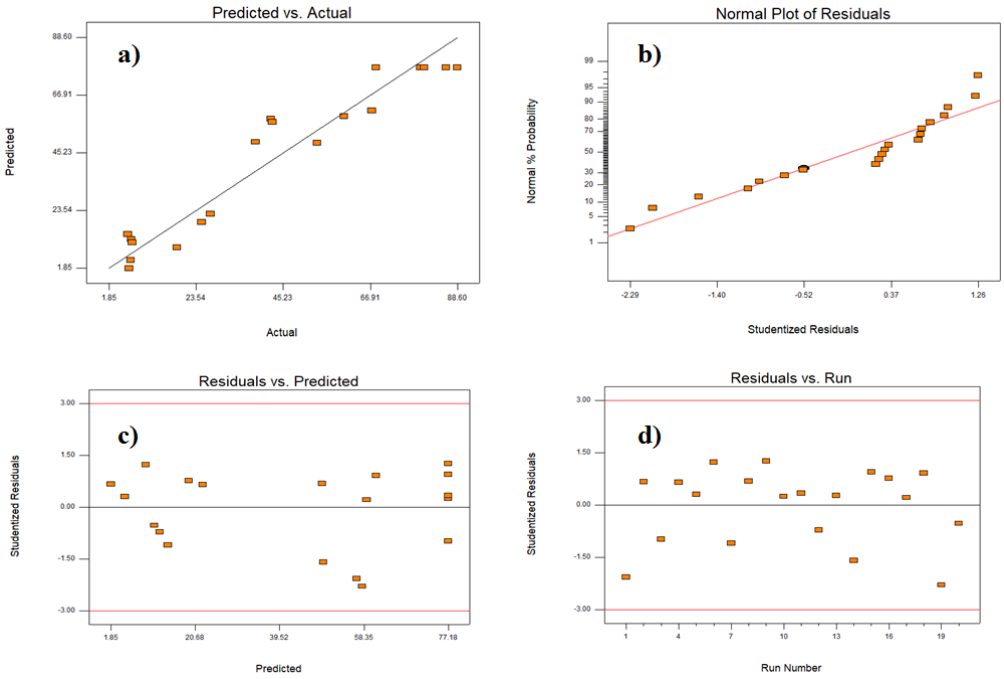

Fig. 9. Diagnostic plot of (a) predicted vs actual value, (b) normal plot of residuals, (c) residuals vs predicted and (d) residuals vs run.

Table 5. Other parameters of statistical value

Standard deviation	9.68	R-Squared	0.9292
Mean	44.63	Adj R-Squared	0.8965
C. V.	21.69	Pred R-Squared	0.7869
PRESS	3667.34	Adeq Precision	13.152

Table 6. Isotherm parameters for Langmuir and Freundlich models

Isotherm model	Langmuir			Freundlich		
Estimated isotherm parameters	Q_{max} (mg/g)	K_L (L/mg)	R^2	$1/n$	K_f (mg/g)	R^2
	14284.71	6.19×10-3	0.9416	1.002	114.76	0.8545

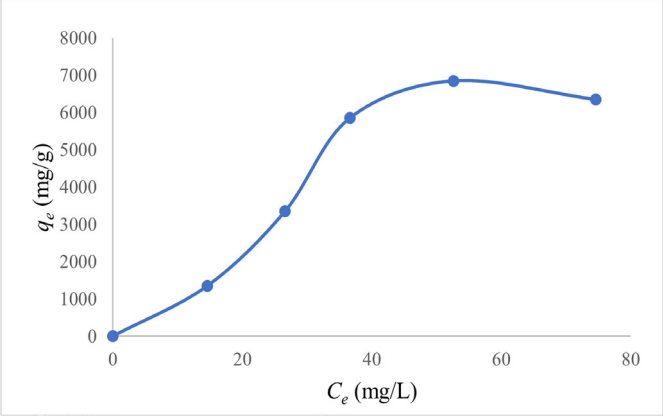

Fig. 10. Equilibrium concentration vs final concentration of arsenic

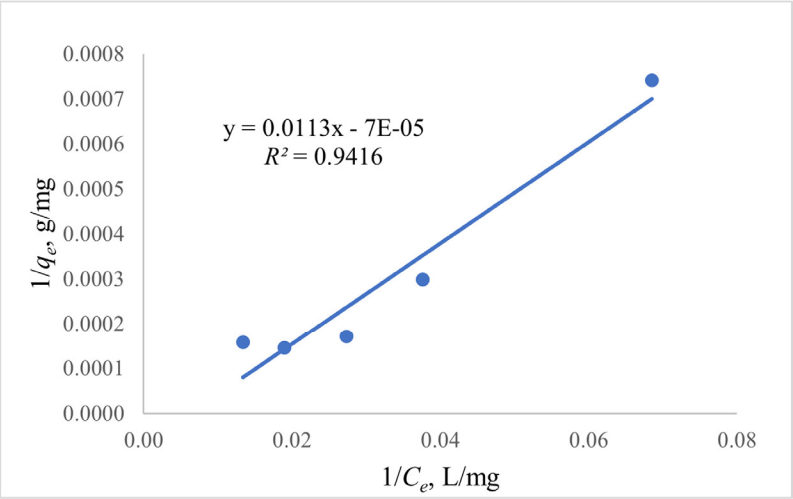

Fig. 11. Langmuir isotherm model

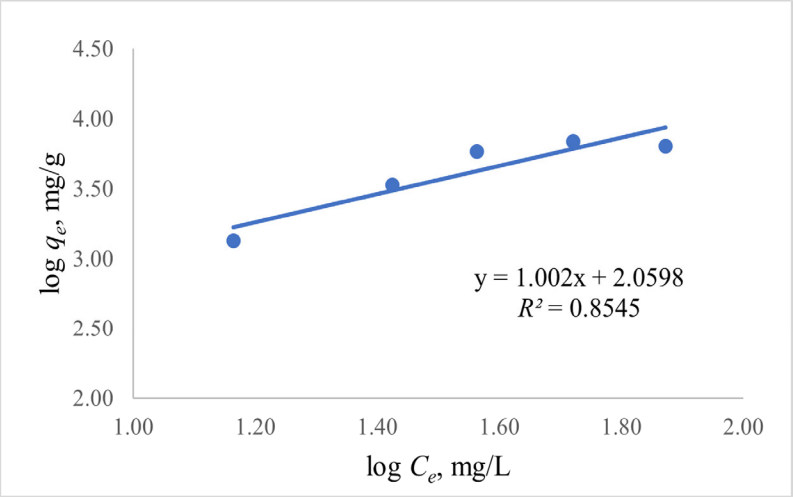

Fig. 12. Freundlich isotherm models

were tabulated in Table 6.

The graph of the equilibrium arsenic concentration versus the arsenic concentration in the solution is shown in Fig. 10. A linear Langmuir adsorption isotherm plot of $1/q_e$ versus $1/C_e$ was presented in Fig. 11. Similarly, Fig. 12 shows the Freundlich linear isotherm plot of log q_e versus log C_e.

From the graph in Fig. 11, the regression value of 0.9416 was determined, which was higher than the value for the Freundlich model (Fig. 12) with a regression value of 0.8545. With R^2 value approaching 1.0, the adsorption process had the best fit with the Langmuir isotherm model with a high maximum adsorption capacity of 14284.21 mg/g. Therefore, the dominating Langmuir isotherm model fit suggested that there were a restricted number of active sites on the surface of the fabricated nanocomposite membrane and a monolayer of arsenic ions formed over the homogeneous composite surface. Previous findings have also reported that nanocomposite adsorbents show a great fit with Langmuir isotherm [52,57].

CONCLUSION

Arsenic removal from synthetic wastewater using PES-GO-PVP nanocomposite membrane via batch adsorption was studied in this work. The highest arsenic percentage removal of 88.6% was observed from the batch adsorption tests carried

out with an initial arsenic concentration of 55 mg/L, pH 8, and a contact time of 75 minutes. The study of the adsorption isotherm model showed that the process had the best fit with the Langmuir isotherm model with a regression value close to 1.0, with R^2 0.9416. The Langmuir fitted model indicated the monolayer adsorption mechanism of arsenic by the fabricated nanocomposite adsorptive membrane. The modification of polymeric membrane with the addition of GO and PVP is an excellent approach to develop an enhanced adsorptive membrane and improved the membrane mechanical properties compared to the bare PES membrane Thus, this study has shown the promising potential of the PES-GO-PVP nanocomposite membrane for removing arsenic from wastewater and could be utilized as an improved wastewater treatment technology for arsenic removal. Therefore, future research on membrane regeneration studies and membrane flux should be conducted to evaluate the cost and practical applicability of this PES-GO-PVP nanocomposite adsorptive membrane.

CONFLICTS OF INTEREST

The authors declare there are no conflicts of interest.

REFERENCES

1. Shaji E, Santosh M, Sarath KV, Prakash P, Deepchand V, Divya BV. Arsenic contamination of groundwater: A global synopsis with focus on the Indian Peninsula. Geoscience Frontiers. 2021;12(3):101079.
2. Karnib M, Kabbani A, Holail H, Olama Z. Heavy Metals Removal Using Activated Carbon, Silica and Silica Activated Carbon Composite. Energy Procedia. 2014;50:113-20.
3. Mukhopadhyay M, Lakhotia SR, Ghosh AK, Bindal RC. Removal of arsenic from aqueous media using zeolite/chitosan nanocomposite membrane. Separation Science and Technology. 2018;54(2):282-8.
4. Ungureanu G, Santos S, Boaventura R, Botelho C. Arsenic and antimony in water and wastewater: Overview of removal techniques with special reference to latest advances in adsorption. Journal of Environmental Management. 2015;151:326-42.
5. Hussain MM, Wang J, Bibi I, Shahid M, Niazi NK, Iqbal J, et al. Arsenic speciation and biotransformation pathways in the aquatic ecosystem: The significance of algae. Journal of Hazardous Materials. 2021;403:124027.
6. Gunatilake SK. Methods of Removing Heavy Metals from Industrial Wastewater. 2015;1(1):12–8.
7. Azimi A, Azari A, Rezakazemi M, Ansarpour M. Removal of Heavy Metals from Industrial Wastewaters: A Review. ChemBioEng Reviews. 2017;4(1):37-59.
8. Carolin CF, Kumar PS, Saravanan A, Joshiba GJ, Naushad M. Efficient techniques for the removal of toxic heavy metals from aquatic environment: A review. Journal of Environmental Chemical Engineering. 2017;5(3):2782-99.
9. Lai, Soon Onn;Chong, Kok Chung; Kerk, Zhi Wei; Ooi, Boon Seng; Lau WJ. Fabrication Of Pes/Mno Mixed Matrix Membranes For Cadmium Removal. Malaysian J Anal Sci. 2017;21(2):381–90.
10. Imran M, Iqbal MM, Iqbal J, Shah NS, Khan ZUH, Murtaza B, et al. Synthesis, characterization and application of novel MnO and CuO impregnated biochar composites to sequester arsenic (As) from water: Modeling, thermodynamics and reusability. Journal of Hazardous Materials. 2021;401:123338.
11. Iqbal J, Shah NS, Sayed M, Imran M, Muhammad N, Howari FM, et al. Synergistic effects of activated carbon and nano-zerovalent copper on the performance of hydroxyapatite-alginate beads for the removal of As3+ from aqueous solution. Journal of Cleaner Production. 2019;235:875-86.
12. Khulbe KC, Matsuura T. Removal of heavy metals and pollutants by membrane adsorption techniques. Applied Water Science. 2018;8(1).
13. Obotey Ezugbe E, Rathilal S. Membrane Technologies in Wastewater Treatment: A Review. Membranes. 2020;10(5):89.
14. Santhosh C, Velmurugan V, Jacob G, Jeong SK, Grace AN, Bhatnagar A. Role of nanomaterials in water treatment applications: A review. Chemical Engineering Journal. 2016;306:1116-37.
15. Zhao M, Xu Y, Zhang C, Rong H, Zeng G. New trends in removing heavy metals from wastewater. Applied Microbiology and Biotechnology. 2016;100(15):6509-18.
16. Burakov AE, Galunin EV, Burakova IV, Kucherova AE, Agarwal S, Tkachev AG, et al. Adsorption of heavy metals on conventional and nanostructured materials for wastewater treatment purposes: A review. Ecotoxicology and Environmental Safety. 2018;148:702-12.
17. Yoon Y, Park WK, Hwang T-M, Yoon DH, Yang WS, Kang J-W. Comparative evaluation of magnetite–graphene oxide and magnetite-reduced graphene oxide composite for As(III) and As(V) removal. Journal of Hazardous Materials. 2016;304:196-204.
18. Yu B, Huang Q, Liu Y, Jiang G. Fabrication of composite biofibres based on chitosan and fluorinated graphene for adsorption of heavy metal ions in water. The Journal of The Textile Institute. 2018;110(3):426-34.
19. Alenazi NA, Hussein MA, Alamry KA, Asiri AM. Modified polyether-sulfone membrane: a mini review. Designed Monomers and Polymers. 2017;20(1):532-46.
20. Peydayesh M, Bagheri M, Mohammadi T, Bakhtiari O. Fabrication optimization of polyethersulfone (PES)/polyvinylpyrrolidone (PVP) nanofiltration membranes using Box–Behnken response surface method. RSC Advances. 2017;7(40):24995-5008.
21. Amin PD, Bhanushali V, Joshi S. Role of Polyvinlyppyrrolidone in Membrane Technologies. International Journal of ChemTech Research. 2018;11(9):247-59.
22. Mahmoudi E, Ang WL, Ng CY, Ng LY, Mohammad AW, Benamor A. Distinguishing characteristics and usability of graphene oxide based on different sources of graphite feedstock. Journal of Colloid and Interface Science. 2019;542:429-40.
23. Junaidi NFD, Othman NH, Shahruddin MZ, Alias NH, Lau WJ, Ismail AF. Effect of graphene oxide (GO) and polyvinylpyrollidone (PVP) additives on the hydrophilicity of composite polyethersulfone (PES) membrane. Malaysian Journal of Fundamental and Applied Sciences.

2019;15(3):361-6.
24. Nik-Abdul-Ghani NR, Jami MS, ENgliman NS, AMosa MK, Isa MH. Study of graphene oxide-polymer nanocomposite (GPN) adsorptive membrane for lead removal from wastewater (in press). Journal of Engineering Science & Technology (JESTEC). 2021.
25. Chen X. Modeling of Experimental Adsorption Isotherm Data. Information. 2015;6(1):14-22.
26. Ramesha GK, Vijaya Kumara A, Muralidhara HB, Sampath S. Graphene and graphene oxide as effective adsorbents toward anionic and cationic dyes. Journal of Colloid and Interface Science. 2011;361(1):270-7.
27. Zaaba NI, Foo KL, Hashim U, Tan SJ, Liu W-W, Voon CH. Synthesis of Graphene Oxide using Modified Hummers Method: Solvent Influence. Procedia Engineering. 2017;184:469-77.
28. Krishnamoorthy K, Veerapandian M, Yun K, Kim SJ. The chemical and structural analysis of graphene oxide with different degrees of oxidation. Carbon. 2013;53:38-49.
29. Amosa MK, Jami MS, Alkhatib MaFR. Electrostatic Biosorption of COD, Mn and H2S on EFB-Based Activated Carbon Produced through Steam Pyrolysis: An Analysis Based on Surface Chemistry, Equilibria and Kinetics. Waste and Biomass Valorization. 2015;7(1):109-24.
30. Fraga TJM, Carvalho MN, Ghislandi MG, Motta Sobrinho MAd. FUNCTIONALIZED GRAPHENE-BASED MATERIALS AS INNOVATIVE ADSORBENTS OF ORGANIC POLLUTANTS: A CONCISE OVERVIEW. Brazilian Journal of Chemical Engineering. 2019;36(1):1-31.
31. Thema FT, Moloto MJ, Dikio ED, Nyangiwe NN, Kotsedi L, Maaza M, et al. Synthesis and Characterization of Graphene Thin Films by Chemical Reduction of Exfoliated and Intercalated Graphite Oxide. Journal of Chemistry. 2013;2013:1-6.
32. Junaidi NFD, Othman NH, Shahruddin MZ, Alias NH, Marpani F, Lau WJ, et al. Fabrication and characterization of graphene oxide–polyethersulfone (GO–PES) composite flat sheet and hollow fiber membranes for oil–water separation. Journal of Chemical Technology & Biotechnology. 2020;95(5):1308-20.
33. Johra FT, Lee JW, Jung WG. Facile and safe graphene preparation on solution based platform. J Ind Eng Chem. 2014;20(5):2883–7.
34. Blanton TN, Majumdar D. X-ray diffraction characterization of polymer intercalated graphite oxide. Powder Diffraction. 2012;27(2):104-7.
35. Kim C-D, Min B-K, Jung W-S. Preparation of graphene sheets by the reduction of carbon monoxide. Carbon. 2009;47(6):1610-2.
36. Shen L, Zhang L, Wang K, Miao L, Lan Q, Jiang K, et al. Analysis of oxidation degree of graphite oxide and chemical structure of corresponding reduced graphite oxide by selecting different-sized original graphite. RSC Advances. 2018;8(31):17209-17.
37. Shao G, Lu Y, Wu F, Yang C, Zeng F, Wu Q. Graphene oxide: the mechanisms of oxidation and exfoliation. Journal of Materials Science. 2012;47(10):4400-9.
38. Smith AT, Marie A, Zeng S, Liu B, Sun L. Nano Materials Science Synthesis , properties , and applications of graphene oxide / reduced graphene oxide and their nanocomposites. Nano Mater Sci . 2019;1(1):31–47.
39. Rattana, Chaiyakun S, Witit-anun N, Nuntawong N, Chindaudom P, Oaew S, et al. Preparation and characterization of graphene oxide nanosheets. Procedia Engineering. 2012;32:759-64.
40. Yusoff Y, Samad S, Loh KS, Lee TK. Structural and Morphological Study of Sulfonated Graphene Oxide Prepared with Different Precursors. 2018;1(2):65–71.
41. Alam J, Shukla AK, Alhoshan M, Arockiasamy Dass L, Muthumareeswaran MR, Khan A, et al. Graphene oxide, an effective nanoadditive for a development of hollow fiber nanocomposite membrane with antifouling properties. Advances in Polymer Technology. 2018;37(7):2597-608.
42. Peng W, Li H, Liu Y, Song S. A review on heavy metal ions adsorption from water by graphene oxide and its composites. Journal of Molecular Liquids. 2017;230:496-504.
43. Sitko R, Turek E, Zawisza B, Malicka E, Talik E, Heimann J, et al. Adsorption of divalent metal ions from aqueous solutions using graphene oxide. Dalton Transactions. 2013;42(16):5682.
44. Abdel-Karim A, Gad-Allah TA, El-Kalliny AS, Ahmed SIA, Souaya ER, Badawy MI, et al. Fabrication of modified polyethersulfone membranes for wastewater treatment by submerged membrane bioreactor. Separation and Purification Technology. 2017;175:36-46.
45. Nguyen HTV, Ngo THA, Do KD, Nguyen MN, Dang NTT, Nguyen TTH, et al. Preparation and Characterization of a Hydrophilic Polysulfone Membrane Using Graphene Oxide. Journal of Chemistry. 2019;2019:1-10.
46. Kotsilkova R, Borovanska I, Todorov P, Ivanov E, Menseidov D, Chakraborty S, et al. Tensile and Surface Mechanical Properties of Polyethersulphone (PES) and Polyvinylidene Fluoride (PVDF) Membranes. Journal of Theoretical and Applied Mechanics. 2018;48(3):85-99.
47. Mataram A, Rizal S, Saputra RA. Characteristics of polyethersulfone membranes with the addition of silver nitrate ; tensile strength , microstructure , and permeability Characteristics of Polyethersulfone Membranes with the Addition of Silver Nitrate ; Tensile Strength , Microstructure. AIP Conf Proc. 2019;020041(2129 (020041)):1–5.
48. Alkindy MB, Naddeo V, Banat F, Hasan SW. Synthesis of polyethersulfone (PES)/GO-SiO2 mixed matrix membranes for oily wastewater treatment. Water Science and Technology. 2019;81(7):1354-64.
49. Kadhim RJ, Al-Ani FH, Al-shaeli M, Alsalhy QF, Figoli A. Removal of Dyes Using Graphene Oxide (GO) Mixed Matrix Membranes. Membranes. 2020;10(12):366.
50. Wang Y, Liu X, Huang Y, Hayat T, Alsaedi A, Li J. Interaction mechanisms of U(VI) and graphene oxide from the perspective of particle size distribution. Journal of Radioanalytical and Nuclear Chemistry. 2016;311(1):209-17.
51. Shahrin S, Lau W-J, Goh P-S, Ismail AF, Jaafar J. Adsorptive mixed matrix membrane incorporating graphene oxide-manganese ferrite (GMF) hybrid nanomaterial for efficient As(V) ions removal. Composites Part B: Engineering. 2019;175:107150.
52. Joshi S, Sharma M, Kumari A, Shrestha S. applied sciences Arsenic Removal from Water by Adsorption onto Iron Oxide / Nano-Porous Carbon Magnetic Composite.
53. Rahdar S, Taghavi M, Khaksefidi R, Ahmadi S. Adsorption of arsenic (V) from aqueous solution using modified saxaul ash: isotherm and thermodynamic study. Applied Water

Science. 2019;9(4).
54. Gaur N, Kukreja A, Yadav M, Tiwari A. Adsorptive removal of lead and arsenic from aqueous solution using soya bean as a novel biosorbent: equilibrium isotherm and thermal stability studies. Applied Water Science. 2018;8(4).
55. Nguyen K, Nguyen B, Nguyen H, Nguyen H. Adsorption of Arsenic and Heavy Metals from Solutions by Unmodified Iron-Ore Sludge. Applied Sciences. 2019;9(4):619.
56. Ji K, Xu H, Ma X, Yin J, Jiang X. Hyperbranched poly(ether amine)@poly(vinylidene fluoride) (hPEA@PVDF) porous membranes for selective adsorption and molecular filtration of hydrophilic dyes. Journal of Materials Chemistry A. 2017;5(21):10470-9.
57. Jung Y-J, Kamimoto Y. Arsenic removal properties by electrolyzed and calcined manganese dioxide. Environmental Engineering Research. 2019;25(5):735-41.